Quantitative image analysis of influence of polysaccharides on protein network formation in GDL-acidified milk gels

Food Structure 38 (2023) 100352

Contents lists available at ScienceDirect

Food Structure

journal homepage: www.elsevier.com/locate/foostr

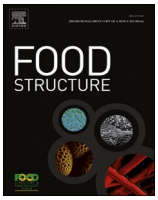

Quantitative image analysis of influence of polysaccharides on protein network formation in GDL-acidified milk gels

Mariska Brüls [a,b], Sanam Foroutanparsa [a,b], Théo Merland [a,b], C. Elizabeth P. Maljaars [c], Maurien M.A. Olsthoorn [d], Roderick P. Tas [a,b], Ilja K. Voets [a,b,*]

[a] Laboratory of Self-Organizing Soft Matter, Department of Chemical Engineering and Chemistry, the Netherlands
[b] Institute for Complex Molecular Systems, Eindhoven University of Technology, P.O. Box 513, 5600 MB Eindhoven, the Netherlands
[c] DSM Food & Beverages, Center for Food Innovation, Alexander Fleminglaan 1, 2613 AX Delft, the Netherlands
[d] DSM Science & Innovation, Biodata & Translational Sciences, Alexander Fleminglaan 1, 2613 AX Delft, the Netherlands

ARTICLE INFO

Keywords:
Acidified milk gel
Polysaccharides
2D spatial autocorrelation analysis
Fourier transform
Rheology

ABSTRACT

Exopolysaccharides (EPS) are commonly used to improve the texture of yogurt. These polysaccharides interact with casein micelles, the major protein in milk, via electrostatic and depletion mechanisms during fermentation by lactic acid bacteria (LAB). However, the relationship between the physicochemical properties and monosaccharide composition of EPS and their impact on yogurt texture is not yet fully understood. To address this knowledge gap, we studied the effects of polysaccharides commonly used as food additives on acid-induced milk protein networks. Confocal laser scanning microscopy (CLSM) was used to image the network microstructures. Image analysis, including Fourier transform, autocorrelation, and binarization-based techniques, was applied to quantify key structural features of the mixed milk protein/polysaccharide gels. These parameters were then related to the macroscopic properties of the model food matrices, such as elastic and viscous moduli and yield point. We found that the addition of neutral polysaccharides resulted in a concentration-dependent increase in structure factor, protein domain size, and pore fraction. In contrast, the presence of charged polysaccharides led to an increase in protein domain size, a decrease in pore fraction, and a decrease in elastic and viscous moduli. These results demonstrate the use of a quantitative image analysis method for selecting LAB with favorable EPS properties to improve yogurt texture.

1. Introduction

The demand for healthy food products that are low-fat and free of synthetic additives has been increasing due to the rising consumer awareness of the importance of good nutrition (Lynch et al., 2018; Metilli et al., 2020). To meet these demands, the food industry must develop products that offer improved nutritional and sensory quality. Achieving these requirements depends on an understanding of the impact of ingredients on food microstructure and the resulting characteristics of the final product (Aguilera, 2005). The microstructure is particularly critical in fermented milk products, such as sour cream, cottage cheese, and yogurt. For these foods, the processing conditions largely affect the final milk gel texture, firmness, and viscosity (John A. Lucey, 2004). Fermented milk products are high in nutritional value and are consumed worldwide, with yogurt being the most popular (Savaiano & Hutkins, 2021; Tamang et al., 2020). During the formation of yogurt, lactic acid bacteria (LAB) convert lactose present in milk into lactic acid (Duboc & Mollet, 2001). The pH decreases as a result, causing destabilization of the casein micelles, which comprise approximately 80% of the protein in bovine milk.

Casein micelles are assemblies of mainly four types of casein proteins (α_{s1}-, α_{s2}-, β-, and κ- caseins) and colloidal calcium phosphate held together by hydrophobic interactions and hydrogen bonding (Lucey & Singh, 1997). The κ-caseins are located on the outer surface of the micelles and stabilize the casein micelles against aggregation by extending its hydrophilic C-terminal moiety, the so-called caseinomacropeptide (CMP) (Dalgleish, 2011). The CMP is hydrophilic and extends away from the casein micelle surface by 5–10 nm, creating a so-called 'hairy layer', which provides steric stabilization. During acidification of milk, the CMP chains loses the intra- and interchain repulsive electrostatic interactions and collapse onto the κ-casein layer (Dalgleish & Corredig, 2012). This decreases the steric stabilization of the micelles, allowing

* Corresponding author at: Laboratory of Self-Organizing Soft Matter, Department of Chemical Engineering and Chemistry, the Netherlands.
E-mail address: i.voets@tue.nl (I.K. Voets).

https://doi.org/10.1016/j.foostr.2023.100352
Received 31 March 2023; Received in revised form 15 September 2023; Accepted 3 October 2023
Available online 5 October 2023

them to aggregate by short-range attractive forces, resulting in a sol-gel transition. The internal structure of the casein micelles also changes upon acidification. When the pH decreases from 6.6 to 5.3, colloidal calcium phosphate (CCP) is released from the interior of the micelles. A further decrease in pH to 4.6, corresponding to the isoelectric point (pI) of caseins, results in aggregation and gelation. The microstructure of the final yogurt network now consists of an aggregated casein protein network with embedded fat globules and voids filled with serum with soluble proteins, lactose, bacterial cells and excreted metabolites (Duboc & Mollet, 2001). The yogurt microstructure highly depends on the fermentation process and the ingredient composition, and in turn the microstructure leads to specific physical and sensory properties (Sodini et al., 2004). Therefore, it is important to understand how to tune yogurt microstructure by optimizing the fermentation parameters.

An interesting aspect of LAB with regards to yogurt fermentation is the ability of certain LAB strains to produce and secrete polysaccharides (Hassan, 2008). These polysaccharides include exopolysaccharides (EPS) that are released into the surrounding medium and capsular polysaccharides (CPS) that remain attached to the cell wall. Because of the diverse impact polysaccharides have on the casein micelle network structure, EPS can be used to enhance yogurt texture naturally without using additives. EPS can influence the formation of casein gels by interfering with protein-protein interactions (Hassan, 2008), facilitate the formation of serum channels and pores during gelation (Lynch et al., 2018), but also increase the compactness of the casein network (Everett & McLeod, 2005) and either reduce (Zhang et al., 2016) or increase (Tiwari et al., 2021) the water holding capacity.

The impact of a specific exopolysaccharide (EPS) on the microstructure of yogurt is influenced by multiple factors, including monosaccharide composition, molecular mass, branching, stiffness, charge density, and their interactions with milk proteins (Mende et al., 2016). Previous research on commercially available polysaccharides has revealed general trends (Corredig et al., 2011; Syrbe et al., 1998) and their underlying physical mechanisms (Kruif & Tuinier, 2001; Turgeon & Laneuville, 2009), including their effects on network formation driven by depletion (Fig. 1A) or bridging (Fig. 1B). Below the isoelectric pH of the caseins, anionic polysaccharides are attracted to the oppositely charged casein micelles (now cationic), leading to bridging flocculation and destabilization of the casein dispersions when the polysaccharide concentration is low. The compactness of the aggregates increases with the number of protein-polysaccharide interactions, and denser structures can form with higher numbers of opposite charges (Turgeon & Laneuville, 2009). Electrostatic interactions with anionic polysaccharides also strengthen the final protein network (Everett & McLeod, 2005) and result in smaller pores (Loeffler et al., 2020). However, if the biomacromolecules have low affinity for each other, the mixture may destabilize in a segregative manner through depletion, generating domains enriched in either biomacromolecule and depleted of the other. This applies to mixtures of neutral polysaccharides and casein micelles. Non-adsorbing neutral polysaccharides and excess anionic polysaccharides increase serum viscosity (Everett & McLeod, 2005) and can accelerate casein aggregation by depletion effects (Kruif & Tuinier, 2001). Stiffer polysaccharide chains may also enhance protein aggregation. Rigid polysaccharides may bind weaker to oppositely charged proteins, because chain rigidity may not afford sufficient conformational flexibility to reach oppositely charged patches on the protein in an optimal manner (Kayitmazer et al., 2003). Laneuville and Turgeon observed that xanthan and k-carrageenan, both having high chain stiffness, induce segregative phase separation and induce syneresis in acidified milk gels (Laneuville & Turgeon, 2014). An increase in branching (Tuinier et al., 2001) and charge density (Zdunek & Pieczywek, 2021) both increase the stiffness of polysaccharide chains.

Previous studies have investigated the interaction between milk proteins and a selection of specific in-situ produced EPS (Ayala--Hernandez et al., 2008; Gentès et al., 2013), isolated EPS (Girard & Schaffer-Lequart, 2008; Weinbreck et al., 2003) and polysaccharides (Buldo et al., 2016). However, quantitative approaches have not yet been utilized to study the effect of EPS and polysaccharides on the microstructure of mixed milk protein/exopolysaccharide gels. Several quantitative image analysis techniques have been applied to yogurt

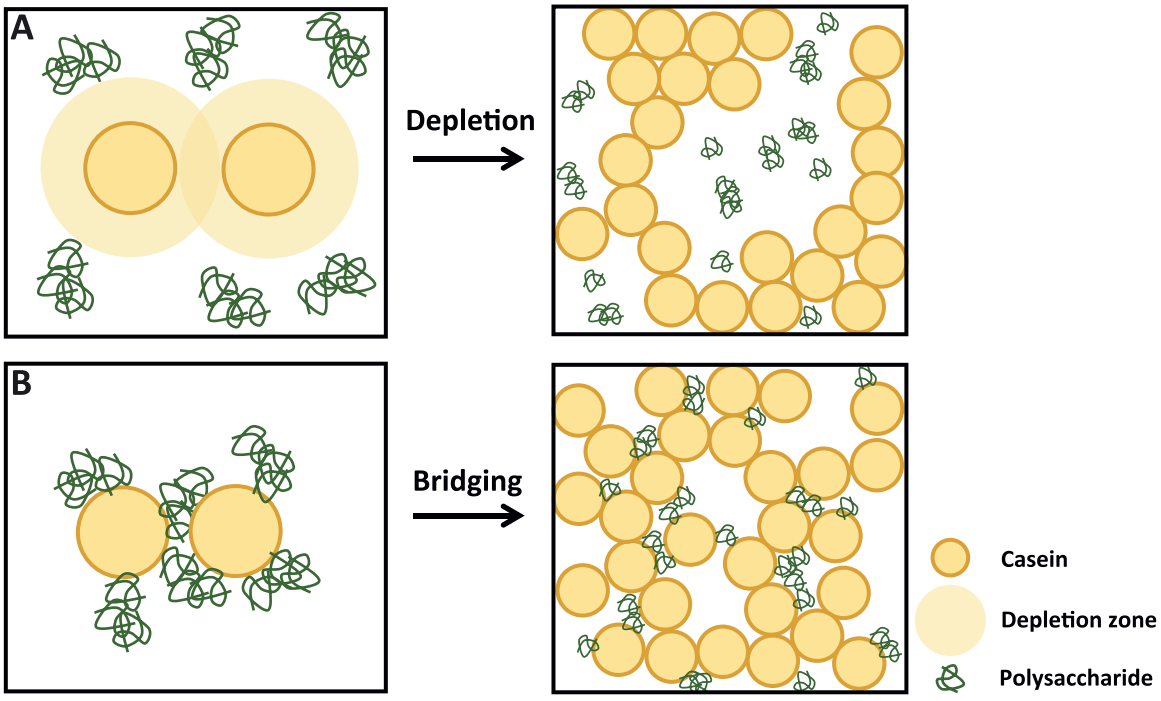

Fig. 1. Schematic overview of polysaccharide/casein interaction modes and their consequences for the formation and structure of milk protein gels. A) Non-adsorbing neutral and excess anionic polysaccharides can drive casein aggregation by depletion flocculation. B) At low concentration negatively charged, adsorbing polysaccharides can destabilize casein dispersions by bridging flocculation.
Adapted from de Kruif & Tuinier (Kruif & Tuinier, 2001).

microstructure, but these studies did not focus on the effect of EPS and polysaccharides. Analysis techniques that have been utilized include grayscale morphology analysis (Fenoul et al., 2008), typical aggregate size, binarization (Silva et al., 2015), fractal image analysis (Torres et al., 2012), Fourier transform and autocorrelation based image analysis (Glover et al., 2019) to assess various structural features of milk protein gels, such as fractal dimension, protein domain size and pore fraction.

Since EPS produced by different LAB strains differ greatly in chemical composition and physical properties (Birch et al., 2019), it is crucial to quantitatively analyze the microstructure of mixed milk protein/exopolysaccharide gels to achieve a detailed, fundamental understanding of EPS structure-yoghurt property relations. Whilst the rate and (local) concentration of LAB produced EPS is largely unknown, it is important to investigate these properties for a comprehensive series of (E)PS premixed with milk proteins, such that the composition of the milk protein/(exo)polysaccharide mixtures is controlled and known. Whereas in previous work the effect of EPS on microstructure is studied merely qualitatively, in this work we compare and contrast in a quantitative manner the influences of different commercially-used polysaccharides, with known composition and physical properties, on gelation in yogurt model systems, comprising mixtures of polysaccharides and milk protein concentrate powder (MPC) acidified by D-(+)-gluconic acid δ-lactone (GDL). We compared the effect on microstructure of polysaccharides that vary in charge density, hydrophilicity, chain flexibility and propensity to aggregate and form helices. Specifically, we focused on low acyl gellan (LAG), high acyl gellan (HAG), xanthan, guar gum and ι-carrageenan. We analyzed CLSM images from acidified milk gels containing these different types of polysaccharides to determine the structure factor, average protein domain size and pore fraction. This approach allows us to relate differences in microstructure induced by the various polysaccharides and imaged by CLSM to variations in the viscoelasticity of the network determined by rheometry.

2. Materials and methods

2.1. Materials

Milk protein concentrate powder containing 80 wt% protein (MPC80) was kindly provided by the Hungarian Dairy Research Institute Ltd. During MPC80 powder preparation, milk was subjected to ultrafiltration and subsequent diafiltration to exclusively concentrate protein and casein-bound CaP (Babella, 1989). The retentate was heat treated by direct steam infusion at 130 °C for 20 s, followed by vacuum evaporation and spray-drying. The composition of the resulting MPC80 powder was 80% milk proteins (comprising a casein-to-whey protein ratio of 80:20, which is similar to the natural ratio in milk), 7.5% ash, 5.5% lactose, 5% water and 1.5% fat. LAG, HAG, xanthan, and yeast extract were kindly provided by DSM Biotechnology Center (Delft, The Netherlands). Guar gum, ι-carrageenan (commercial grade, type II), rhodamine B and D-(+)-gluconic acid δ-lactone (GDL, ≥99.0%) were purchased from Merck. Fresh pasteurized skimmed milk (fat content < 0.1%, de Zaanse Hoeve) was locally purchased in the Netherlands. All compounds were used as received. Characteristics of the commercially available polysaccharides used in this study, as reported in literature, are listed in Table 1. A more extensive comparison of the properties of the polysaccharides, also based on information available from the literature, is given in the supplementary information (S1). In brief, low acyl gellan is produced from high acyl gellan by removal of the acetate and glycerate moieties (Buldo et al., 2016). HAG is less prone to aggregation compared to LAG since its acyl groups interfere with aggregation of double helices. As a result, LAG forms hard brittle gels whereas HAG forms soft elastic gels (Williams & Phillips, 2003). Xanthan has the same charge density as LAG and HAG but has a trisaccharide sidechain

Table 1
Overview the PS and their composition, charge density and structure.

Polysaccharide	Composition[a]	Molecular Weight (kg/mol)[i]	Persistence Length (nm)	Charge density[a]	Structure[b,c]
Low acyl gellan	Linear chain of glucuronic acid (◇), glucose (●) and rhamnose (▲) in the ratio 1: 2: 1.	$2.5\bullet10^2$	70–100[d]	0.25	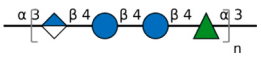
High acyl gellan	Linear chain of glucuronic acid with acetyl (OAc) and L-glyceryl as side-groups (Williams & Phillips, 2003), glucose and rhamnose in the ratio 1: 2: 1.	$1.5\bullet10^3$	25[e]	0.25	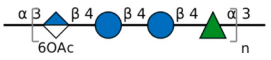
Xanthan	Glucose backbone with trisaccharide side-chain of mannose, glucuronic acid and mannose with acetyl and pyruvate (Pyr) substituents.	$1.5\bullet10^3$	125[f]	0.25	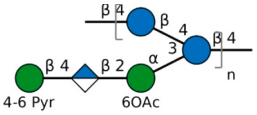
Guar	Mannose backbone with galactose (●) as monosaccharide side-chain.	$1.5\bullet10^3$	10[g]	0	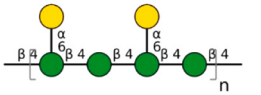
ι-carrageenan	Linear chain of galactose and anhydrogalactose (◇), with a sulphate group (S) on every saccharide.	$1.5\bullet10^3$	23[h]	1	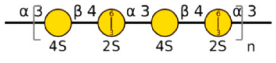

[a] (de Jong & van de Velde, 2007),
[b] (Cheng et al., 2017),
[c] Schematically depicted using the standardized Symbol Nomenclature For Glycans (SNFG). The configurations (α/β) and position of the glycosidic linkages are indicated.
[d] (Rinaudo & Milas, 2000),
[e] (Jamil et al., 2019),
[f] (Marguerite, 2001),
[g] (Morris et al., 2008),
[h] (Schefer et al., 2014).
[i] Molecular weights (MW) of low acyl gellan and high acyl gellan were determined by the supplier, the MW for xanthan, guar and ι-carrageenan were determined from static light scattering as described in the supplementary information (S2).

attached to every other monosaccharide unit in the backbone. Guar has a smaller, monosaccharide sidechain and is neutral, in contrast to ι-carrageenan which bears a negative charged sulphate group on every monosaccharide unit in the linear backbone.

2.2. Methods

2.2.1. Preparation of a GDL induced MPC80 gel

The yogurt model system was prepared based on the methods described by Zhang et. al. (Zhang et al., 2015). MPC80 powder was reconstituted to 5.6 wt% (4.5 wt% protein) in MilliQ water and no (control) or 0.04 wt% polysaccharide (LAG, HAG, xanthan, guar gum, ι-carrageenan) was added. This concentration was selected since the protein network is continuous for all studied polysaccharides up until this concentration (de Jong & van de Velde, 2007). The mineral content of the polysaccharides, which is unknown, is assumed to be of negligible importance at this polysaccharide concentration, which is much lower than the MPC concentration (with known mineral content). The resulting reconstituted milk was heated in a thermomixer (Eppendorf® ThermoMixer® C) with mild agitation (300 rpm) for 20 min at 90 °C and subsequently cooled in ice water for 30 min. Sodium azide (0.02 wt %) was added as an antimicrobial agent and the protein was labelled with rhodamine B (0.1 μg/ml), which binds strongly to proteins. The samples are equilibrated to room temperature, subsequently 3.5 wt% GDL was added, and part of the sample was quickly transferred to a chambered microscopy slide (chamber volume = 20 μl). Note that polysaccharide addition has a negligible impact on the rate of pH decline (de Jong & van de Velde, 2007; Sone et al., 2022). As determined by pH monitoring of the remaining sample volume, after incubation for 2 h the pH was 4.3, which below the pI of casein. At this time after GDL addition, five images of the final network structure were taken per sample, and six repetitions are performed for each polysaccharide. Therefore, for each polysaccharide a total of 30 images of milk gel microstructures are analysed.

2.2.2. Confocal laser-scanning microscopy

Confocal laser-scanning microscopy (CLSM, Leica SP8) was performed in the inverted mode with a 100x oil-immersion objective. The pixel size was set to 80 nm, using 0.75 digital zoom to generate images of 1936 × 1936 pixels. Samples were excited with an incident laser at 552 nm with detection between 565 and 630 nm. All images were taken > 10 μm from the glass interface to avoid boundary anomalies in the gel formation (Glover et al., 2019).

2.2.3. Quantitative data analysis

Analysis of variance (ANOVA) was used to evaluate differences between values of the protein domain size, fractal dimension and pore fraction using multiple comparison of means Tukey Honesty Significant Difference (HSD) test. A significance level of $p < 0.05$ was used.

2.2.3.1. Pore fraction analysis. Prior to image analysis, the images are rescaled to maximize contrast using the automatic brightness adjustment function in ImageJ. Further image analysis was conducted with Python 2 using inbuilt functions for area calculation, Fourier transformation and additional custom-made functions. To calculate the pore fraction, a wiener smoothing filter of 5 × 5 pixels was applied to the images using the SciPy function 'wiener'. Inspired by the work of Pugnaloni et al. (Pugnaloni et al., 2005), images were transformed into 8-bit binary images and thresholded, with the mean grey level as threshold. In this way, any pixel with a grey level above the mean value is considered to belong to the protein network, and any pixel with a grey level below is considered to belong to the voids within the network. The pore fraction was subsequently calculated as the total pore area divided by the total image area.

2.2.3.2. Autocorrelation and Fourier space analysis. The autocorrelation and Fourier space analysis were performed according to a method described by (Glover et al., 2019). The autocorrelation *G(a,b)* of an image is defined as:

$$G(a,b) = \sum_{x=1}^{M}\sum_{y=1}^{N} I(x,y) \bullet I(x-a, y-b) \tag{1}$$

Where M and N are the number of pixels in the height and width, respectively, *(a,b)* are the coordinates in the generated autocorrelation image. According to the Wiener-Khinchin theorem (Robertson, 2012), a computationally efficient method to compute the autocorrelation image is to take the inverse Fourier transform of the power spectrum image:

$$S(I) = |\mathscr{F}[I(x,y)]|^2 \tag{2}$$

$$G(a,b) = \mathscr{F}^{-1}[S(I)] \tag{3}$$

Where *S(I)* is the power spectrum of the image, and $\mathscr{F}$ represents the Fourier transform and $\mathscr{F}^{-1}$ the inverse of the Fourier transform. The power spectrum describes how the signal is distributed over the spatial frequencies that together form the image. To limit the influence of variations in intensity over the samples, a normalized autocorrelation $g(a,b)$ is computed by subtraction of the mean intensity, and division by the standard deviation of the image:

$$g(a,b) = \frac{1}{\sigma(x,y)^2}\mathscr{F}^{-1}[\mathscr{F}[I(x,y) - \langle I(x,y)\rangle] \bullet \mathscr{F}^{*}[I(x,y) - \langle I(x,y)\rangle]] \tag{4}$$

Where $\sigma(x,y)$ is the standard deviation of the intensity values of the source image *I*, $\mathscr{F}^{*}$ denotes the complex conjugate of the Fourier transform and $\langle I(x,y)\rangle$ is the average intensity in the image. Then, the radial distribution of the autocorrelation and power spectrum images are computed by a costum built python function which calculates for every pixel in the image the distance to the center of the image, and averages the correlation values over the pixels that have the same distance to the center. The radially averaged correlation values were normalized by division by the largest value, which is at the image center. As demonstrated by (Ako et al., 2009), the radially averaged autocorrelation decay can be fit to a stretched exponential:

$$p(r) = C \bullet e^{-\left(\frac{r}{\xi}\right)^{\beta}} \tag{5}$$

Where C is a constant, β is a value between 1 and 2, and ξ is the characteristic length which in this paper was taken as a measure of the protein domain size. The model *p(r)* was fitted to the radial distribution of the autocorrelation image for each microscopy image using the function 'curve_fit' of the open-source Python library SciPy, and the value for the characteristic length ξ is extracted.

The structure factor was determined from the log-log plot of the radially averaged distribution of the power spectrum image *S(q)*. The power spectrum describes the distribution of power over the spatial frequencies that together form the image.

We assume the images can be described as an isotropic fractal Brownian surface (Super & Bovik, 1991). For the global power spectrum of an isotropic fractal Brownian surface, the following relation in Eq. (6) applies:

$$S(q) \propto \left((u^2+v^2)^{\frac{1}{2}}\right)^{-\beta} = q^{-\beta} \tag{6}$$

In which *(u, v)* are two-dimensional frequency coordinates, and the exponent $\beta > 0$ is the structure factor. Therefore, the gradient of the linear region in the *S(q)* log-log plot is the structure factor β. To extract the structure factor β, a high order polynomial fit was applied to the *S(q)* log-log plot and the minimum value of the derivative was taken as the slope $-\beta$ of the linear region.

2.2.4. Rheology

Rheology measurements are performed with a rheometer (Anton Paar GmbH, MCR501) with double gap cylinder geometry (DG26.7-SN188610). GDL induced MPC80 gel samples with no (as a control) or 0.04 wt% polysaccharide (LAG, HAG, xanthan, guar gum or ι-carrageenan) were prepared as described in Section 2.2.1. After storage overnight at 4 °C of the MPC80-polysaccharide samples, 3.5 wt% D-(+)-gluconic acid δ-lactone (GDL, ≥99.0%, Merck) was added. Subsequently, 3.8 ml sample is added to the rheometer and a few oil droplets are added on top to prevent evaporation. After a 2 h waiting time to allow for gel formation at room temperature (20 °C) at rest, the rheological measurements were started. Frequency sweeps were performed across a frequency range of 100–0.1 Hz at a constant strain of 1%. Amplitude sweeps were performed across a strain range of 1–1000% at a constant frequency of 1 Hz. Each system was prepared twice and every prepared sample is measured once. The results are presented as the average of these two rheology measurements.

3. Results and discussion

Aiming to investigate the impact of polysaccharide properties and concentration on the microstructure of milk protein gels, GDL acidified samples were imaged using CLSM (see materials and methods). To quantify the influence of various polysaccharides and quantitatively compare differences in network structure, the CSLM images were subjected to an autocorrelation and Fourier space analysis as described by (Glover et al., 2019) (Fig. 2). These methods yield information on key features of the food matrices, such as protein domain size, pore fraction and the interfacial roughness of the gel strands in the network.

3.1. Microstructure of milk protein gels with commercially available polysaccharides

The network microstructures formed upon GDL acidification in the absence of PS or in the presence of one of LAG, HAG, xanthan, guar and ι-carrageenan have clearly different characteristics. While guar has a network with thick protein strands and large voids, the control has a network of fine protein strands and smaller void spaces. The networks with LAG and HAG have similar voids as the control, but with thicker protein strands. The ι-Carrageenan network also has protein strands of intermediate thickness, but larger voids. Finally, the xanthan network has a dense protein network with both very small and large voids. This is apparent from both a qualitatively inspection of the confocal images (Fig. 3A-F) and from the quantitative analysis (Fig. 3-I). It is also in line with observations on non-acidified renneted milk gel microstructures with 0.025 wt% xanthan and guar reported previously by others (Tan et al., 2007).

Quantitative analysis revealed significant differences in the microstructures of acidified milk with different polysaccharides. Whilst the protein domain size of the milk protein networks without polysaccharides (Fig. 3A) and with LAG (Fig. 3B) are statistically indifferent, the protein domain size significantly increases (PS ≈ LAG < HAG < ι-carrageenan < xanthan < guar) in the presence of all other polysaccharides (Fig. 3G). These differences are not (easily) detectable upon an exclusively qualitative inspection of the confocal images. Instead, quantitative analysis is required to uncover the effect of added polysaccharides on the microstructure of model yoghurt networks. The protein domains are on average largest in gels with guar and xanthan, with a far larger spread in strand thickness in networks with xanthan than with guar. The mean strand thickness in mixed milk protein/guar networks is about 2.5 μm. The average strand thickness of mixed casein/xanthan networks is 1.7 μm, which is considerably lower. Intermediate protein domain sizes of approximately 1 and 1.4 μm are found in networks containing HAG and ι-carrageenan, respectively. None of the analyzed protein domains in gels with HAG are as small as those without polysaccharides or in the presence of LAG. Networks with ι-carrageenan comprise both small- and intermediate-sized domains.

Gels with the neutral, non-adsorbing polysaccharide guar clearly stand out in protein domain size. Both average domain size as well as the sizes of all analyzed domains were larger than the analyzed domain sizes in all other gels, which do not contain neutral polysaccharides. We attribute this finding to enhanced gel coarsening due to depletion

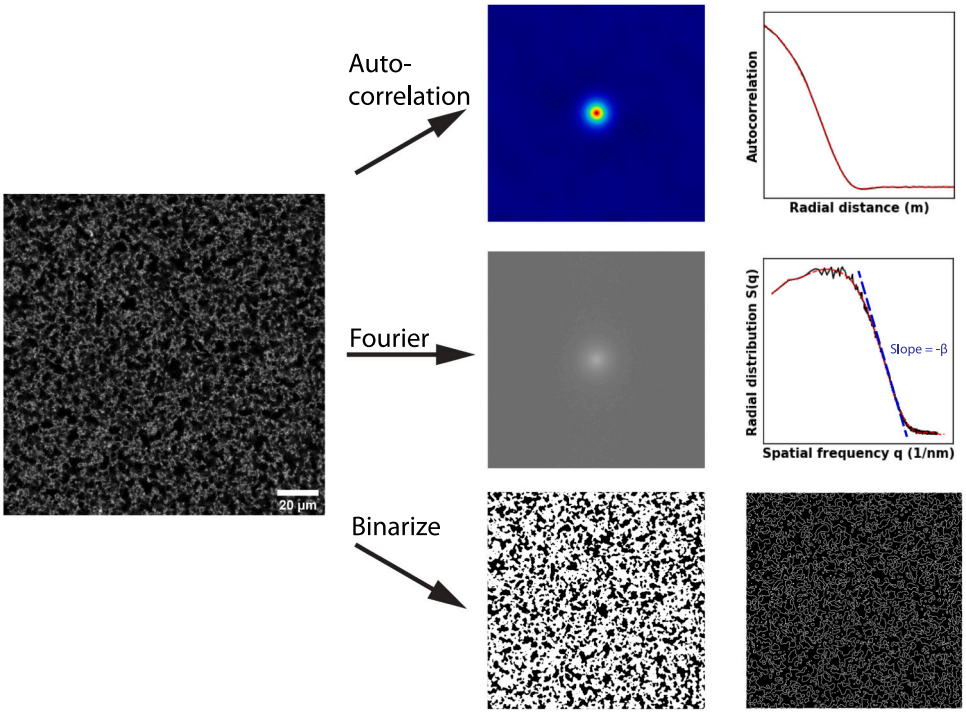

Fig. 2. Overview of the image analysis methods: (top) autocorrelation to calculate the average protein domain size, (middle) Fourier transformation to calculate the structure factor and (bottom) binarization to calculate the pore fraction and pore area distribution.

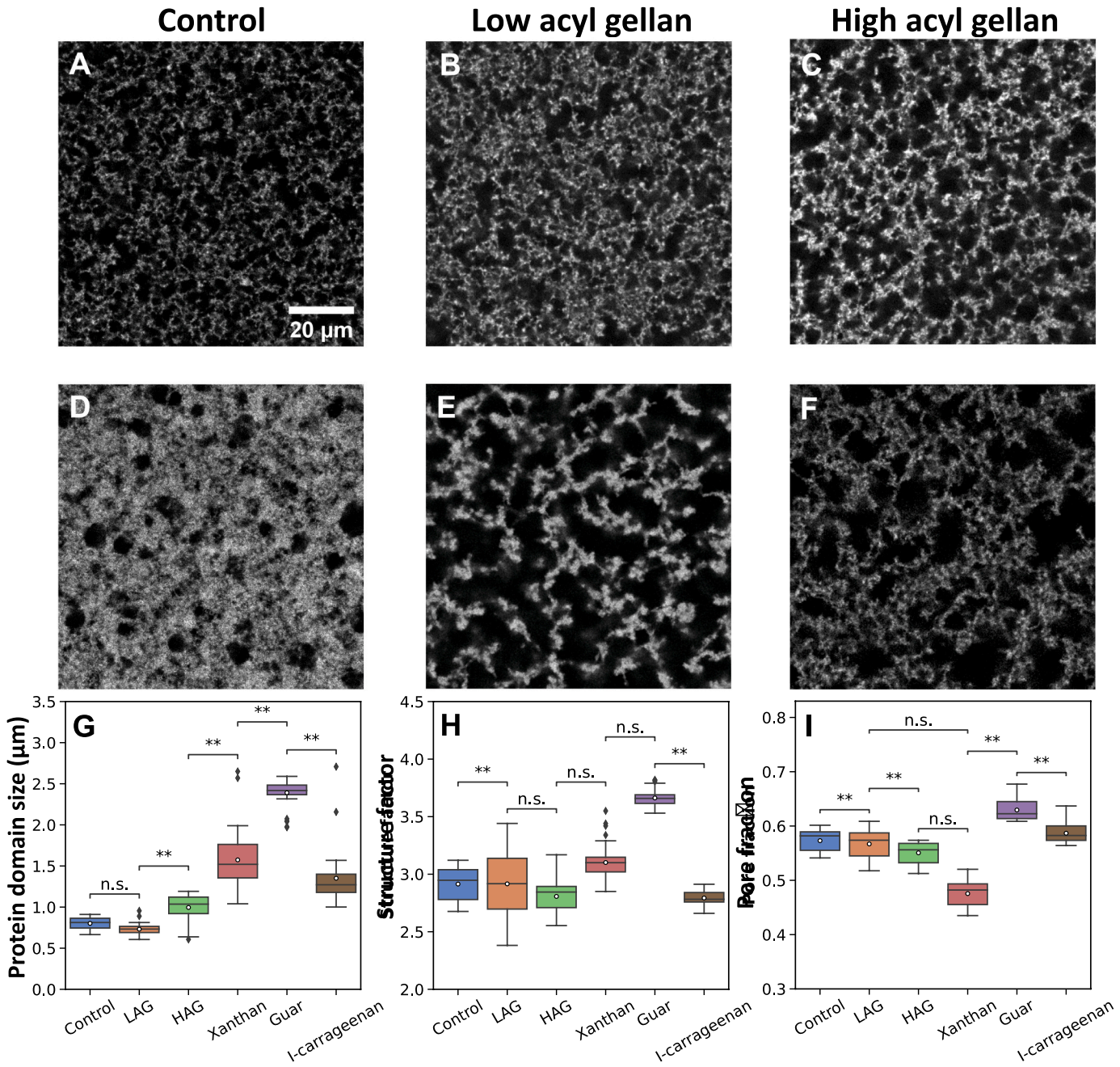

Fig. 3. Confocal images of the protein network microstructure of the GDL-induced milk gel: A) control without polysaccharide, and B) with 0.04 wt% of low acyl gellan, C) high acyl gellan, D) xanthan, E) guar and F) ι-carrageenan. Box plots of G) the protein domain size, H) structure factor and I) pore fraction of the GDL-induced milk gels. Images were taken after 2 h of incubation, at pH 4.3. For samples, the number of images analyzed is n = 30. Statistical significance as calculated with multiple comparison of means Tukey HDS is indicated with asterisks, with not significant (n.s.) for $0.05 < p < 1$, * for $0.01 < p < 0.05$ and * * for $0.001 < p < 0.01$.

interactions arising between the neutral guar and charged casein micelles (Fig. 1A) (Kruif & Tuinier, 2001). In this scenario, it is thermodynamically favorable to minimize the volume excluded to guar, so that its conformation entropy is least compromised. Consequently, a depletion attraction arises between casein micelles, which effectively pushes the milk proteins to aggregate and results in large protein domains interspersed by large pores. Such a coarse microstructure increases the free volume accessible to the polysaccharides and it is therefore entropically more favorable than a network with finer meshes. We observed a similar effect for neutral EPS isolated from lactic acid bacteria, as described in the supplementary information (S3).

Enhanced coarsening may also arise in the four networks containing negatively charged polysaccharides due to bridging interactions at sufficiently low PS concentrations (Fig. 1B) or depletion interactions (sufficiently high concentrations) at pH values below the pI of casein. The branched, low charge density xanthan exhibits the largest impact on protein domain size of all negatively charged PS investigated. Although we cannot directly and unambiguously relate specific microstructural features to the characteristics of the polysaccharides, we believe that this finding is in line with previous work by others showing xanthan having the stiffest chain conformation in milk at neutral pH (Hege et al., 2020). Stiffer chains lead to stronger depletion attractions (Egorov, 2022). Therefore, when present in excess, xanthan exhibits stronger depletion interactions with casein micelles (partially) decorated with

adsorbed xanthan chains resulting in enhanced coarsening. The effect on protein domain size of ι-carrageenan is more pronounced than of LAG and HAG, but less than that of guar and xanthan. As ι-carrageenan has both a high charge density (de Jong & van de Velde, 2007) and a high degree of chain flexibility (Hege et al., 2020), this can likely be attributed to a high level of bridging interactions. An insignificant impact on protein domain size is detected for the linear, low charge density polysaccharide LAG, which may be related to the presence of less acyl groups. Previous studies indicate that the presence of small side groups, such as acyl groups, can interfere with PS-protein interactions (Buldo et al., 2016). Due to the larger number of acyl groups, HAG may cause more depletion interaction than low acyl gellan. We propose that the coarser network with larger protein domain size observed with HAG is due to stronger depletion interactions, caused by the larger number of acyl groups compared to LAG.

Next, we analyzed the structure factor of the gels (Fig. 3H see Section 2.2 for more information). The structure factor is related and inversely proportional to the fractal dimension of the milk gels (Glover et al., 2019). The milk gel microstructure can be modeled as a fractal Brownian surface, and based on the definition of a fractal Brownian surface (Super & Bovik, 1991), a surface with smaller intensity fluctuations, and thus a smoother surface, will have a larger fractal dimension, and thus a smaller structure factor. Vice versa, a rougher surface results in a larger structure factor. Interestingly, it is again the network with guar that stands out most. We find a structure factor of 3.67 ± 0.07, which is higher than that of all other gels without polysaccharide (value) or with anionic polysaccharides (3.10 ± 0.14, 2.91 ± 0.31, 2.81 ± 0.13 and 2.79 ± 0.06 for xanthan, LAG, HAG and ι-carrageenan, respectively. Hence, regardless of charge density, hydrophobicity, and branching density, the microstructures in the presence of the negatively charged polysaccharides all display a comparatively low structure factor. This suggests that the protein-serum interface is smoother in networks with guar than on the other gels. The large spread in the structure factor of the LAG protein network is notable and may be related to a more heterogeneous structure. The spread in domain size is not much larger than for other mixed polysaccharide/milk protein gels (Fig. 3G), but we did observe heterogeneously distributed regions with higher protein density. These correspond to markedly brighter spots in the confocal images of the network. The different polysaccharides also impact the porosity (Fig. 3I). Compared to all the other milk gels, the gels with guar are significantly more porous (with $p < 0.01$) with a total pore fraction of 0.63 ± 0.02. The large pore fractions in the milk gels with guar are expected for a non-adsorbing neutral polysaccharide able to cause strong depletion interactions. In a control experiment, no whey separation was observed in any of the gels, ruling out that the smaller pore fraction of the other gels is due to whey separation (Supplementary Figure S2). The pores in this network appear rather large and interconnected. The smallest pore volume fraction is found in the presence of xanthan (0.48 ± 0.02), whilst all other gels with and without anionic polysaccharides display comparable porosity with pore volume fraction of 0.55 ± 0.02 up to 0.59 ± 0.02. At neutral pH, xanthan-milk solutions at the composition used in this study are unstable and phase separate (Hemar et al., 2001). However, the differences in pore fraction distributions among the images of these gels were not statistically significant.

In summary, the mixed milk protein/polysaccharide network with the neutral polysaccharide guar differs markedly in microstructure from the milk protein gels without polysaccharide and from those with any of the four studied anionic polysaccharides. The guar gel is fairly dense, has a large pore fraction and exhibits a rather smooth protein-serum interface. The negatively charged polysaccharides have more subtle effects on protein domain size, fractal dimension and pore fraction. Differences between these effects are too modest to be appreciated upon qualitative inspection of the confocal images but do become distinguishable upon quantitative analysis.

3.2. Rheological properties of milk protein gels with commercially available polysaccharides

Next, we performed rheometry (Fig. 4) to probe viscoelasticity and yielding. In the linear domain (Fig. 4A, B), all gels display elastic behavior ($G'>G''$) within the studied frequency range. Interestingly, most of the studied polysaccharides impact both G' (Fig. 4A) and G'' (Fig. 4B) in a similar manner. For a direct comparison of the moduli of the different milk gels, we focus on G' and G'' at 1 Hz (Table 2). Whilst the presence of LAG induces an approximately two-fold increase in G' and G'' (to 1210 ± 45 and 310 ± 5 Pa respectively) compared to the gel without polysaccharide (560 ± 6 and 160 ± 3 Pa), HAG and ι-carrageenan decreased the elastic modulus G' and the loss modulus G'' by a factor of 1–2. Sone et al. observed a similarly slight decrease in decrease in G′ and G'' for GDL acidified milk gel with 0.05 wt% ι -carrageenan (Sone et al., 2022). A marked decrease in both G′ and G'' is seen upon addition of xanthan (36 ± 4 and 11 ± 1 Pa, respectively). Strikingly, the addition of guar only slightly increased G′ and G'', to 630 ± 50 and 190 ± 20), whilst mixed milk protein/polysaccharide networks with this neutral polysaccharide display the most pronounced differences in microstructure. Tan et al. observed a larger increase in complex modulus for renneted skim milk gels with similar guar concentration (Tan et al., 2007).

The observed trends in viscoelasticity persist in the non-linear rheology up to moderate strains of 20–25% (Fig. 4C). Yield stress and strain were determined from these experiments, during which an increasingly strong strain was applied to the gels until these finally ruptured. Interestingly, the largest yield strain of $45 \pm 6\%$ and yield stress (140 ± 3 Pa) was found for the gels devoid of polysaccharide (Table 2). Hence, the addition of polysaccharides, neutral as well as anionic, reduces gel toughness and makes the networks more brittle instead. Apart from the gel network with LAG, which was stiffer than the control gel network, globally the control gels were weaker than the gels containing polysaccharides. LAG is known to form brittle gels and to disrupt at lower strain but higher stress compared to HAG gellan (Tong et al., 2018). It ruptured at the same yield stress (140 ± 7 Pa) but two-fold lower yield strain ($22 \pm 3\%$) than the control milk protein gel. In contrast, HAG did not significantly affect the yield strain, but reduced the yield stress to 84 ± 6 Pa. The milk gel with guar had similar yield stress and yield strain as the control milk gel. For xanthan, the yield stress decreased forty-fold to 3 Pa at 28% strain. These findings agree with the reduction in complex modulus for milk gels with 0.025–0.1 wt % xanthan compared to skim milk without polysaccharide, as observed by (Tan et al., 2007). They also observed that xanthan tended to slow down gelation and caused formation of a discontinuous protein network, which likely explains the lower G' and G''. At the composition used in our study, 0.04 wt% and 4.5 wt% milk protein, the xanthan-milk mixture was already thermodynamically incompatible and ready to phase separate at neutral pH (Hemar et al., 2001).

3.3. Relation between rheological properties, gel microstructure and polysaccharide properties

The small yet detectable differences in rheological properties of the mixed polysaccharide/milk protein gels are related in a complex manner to subtle variations in microstructure which in turn originate from differences in the interactions between the various integrated polysaccharides and milk proteins. Although no unambiguous trends were observed between the differences in microstructure and rheological properties, the observations in this study can serve as the basis of future hypotheses on microstructure-function relationships in yogurt. Xanthan does not reinforce the protein network, but rather appears to hinder protein-protein interactions that are essential for the formation of a strong and tough milk protein gel. The low moduli for xanthan-containing gels have been related before to a decrease in the continuity of the protein phase; an effect that becomes more pronounced with

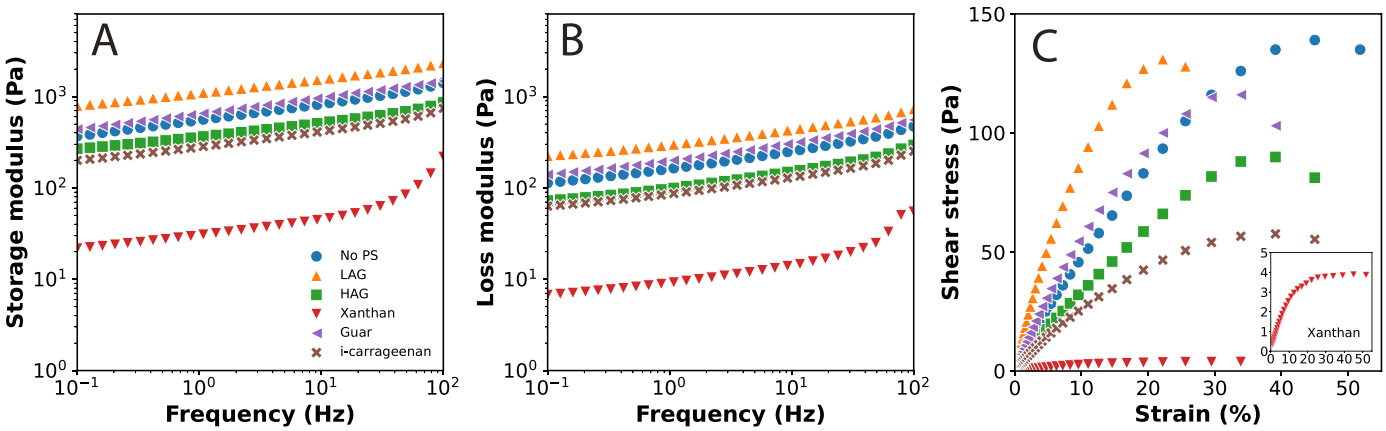

Fig. 4. A) Storage modulus (G'), B) loss modulus (G'') as function of frequency and C) shear stress as a function of strain for GDL-induced milk gel without polysaccharide (blue circles), and with 0.04 wt% of low acyl gellan (orange triangles pointing upwards), high acyl gellan (green squares), xanthan (red triangles pointing downwards), guar (purple triangles pointing to left) and ι-carrageenan (brown crosses).

Table 2
Rheological properties of the milk gels: Storage modulus and loss modulus at 1 Hz and 1% strain, and the yield stress and yield strain. All measurements were performed in duplicate; the reported values denote the mean with accompanying standard deviation.

Polysaccharide	Storage modulus (Pa)	Loss modulus (Pa)	Yield Stress (Pa)	Yield strain (%)
No polysaccharide	560 ± 6	160 ± 3	140 ± 3	45 ± 6
Low acyl gellan	1210 ± 45	310 ± 5	140 ± 7	22 ± 3
High acyl gellan	390 ± 2	110 ± 7	84 ± 6	39 ± 6
Xanthan	36 ± 4	11 ± 1	3 ± 0.5	28 ± 10
Guar	630 ± 50	190 ± 20	130 ± 10	40 ± 6
ι-carrageenan	270 ± 40	83 ± 10	50 ± 10	34 ± 5

increasing polysaccharide concentration (de Jong & van de Velde, 2007). Whether the low moduli are also related to the rather low pore volume fraction is still to be uncovered. The low pore fraction does not seem to be caused by syneresis, since no syneresis was observed (Supplementary information S4). The larger G' and G'' values and brittleness of the low acyl gellan gel are possibly related to its strong interaction with calcium ions (Sworn & Stouby, 2021) and casein (Buldo et al., 2016). and to the presence of non-uniformly distributed dense protein domains, which give rise to the large spread in structure factor. High acyl gellan and ι-carrageenan have similar G' and G'', protein domain size and structure factor. Arguably most striking is the similarity in rheological properties of the gel without any polysaccharide and the guar gel, while their microstructures greatly differ. The guar gel has slightly yet significantly higher moduli than the pristine gel, has a higher porosity, a larger structure fraction and a larger protein domain size. These microstructural differences may have opposing effects on the rheological properties, such that their combined effect is small. Alternatively, their impact may be attenuated by other factors such as the increased guar concentration in the serum due to depletion-induced phase separation in these mixtures comprising neutral polysaccharides and milk proteins. Similarly, van der Velde et al. observed significant differences in whey-gel microstructure at 0 and 0.05 wt% guar, yet at this concentration the guar had little impact on Young modulus (de Jong & van de Velde, 2007). Interestingly, they observed the highest Young modulus at a guar concentration when the pore fraction is largest. To conclusively relate the microstructure characteristics to the rheological properties, the present study could be extended to different polysaccharide concentrations.

4. Conclusions

The influence of different polysaccharides on the microstructure and rheological properties of yogurt model systems has been quantified in mixtures of food grade polysaccharides and milk protein concentrate acidified by GDL. The addition of polysaccharides with varying composition, charge density and branching density resulted in milk gels with distinct microstructures and rheological properties. Quantitative image analysis of CLSM images of these acidified milk gels yielded the structure factor, average protein domain size and pore fraction as parameters to describe the key features of the microstructure. Through this multi-parameter, quantitative image analysis approach, the influence of various polysaccharides on the milk gel microstructure could be differentiated, even if these were not directly apparent from visual inspection by eye. We found that the addition of the neutral polysaccharide guar had the least impact on the rheological properties of the acidified milk protein gels even though these networks have a larger structure factor, larger protein domain size and larger pore fraction compared to networks with negatively charged polysaccharides. Subtle differences in microstructure were detectable in networks containing different negatively charged polysaccharides, presumably originating from variations in their interactions with the milk proteins in the gels. A high degree of acylation, high branching density and high charge density increased protein domain size and weakened the gel network. In future, the presented methodology can also be employed in time-resolved studies to monitor the development of the microstructure and rheological properties of the network. This would reveal when the gels in the presence and absence of various polysaccharides develop characteristic differences and how their formation pathways relate to the final network microstructures and their rheological properties. Another interesting avenue of future research is multi-color imaging of mixed gels with both the proteins and polysaccharides specifically labelled to elucidate the extent to which these are locally mixed and how this relates to network structure and properties.

Declaration of Competing Interest

The authors declare that they have no known competing financial interests or personal relationships that could have appeared to influence the work reported in this paper.

Data availability

Data will be made available on request.

Acknowledgements

This publication is part of the project Localbiofood (with project number 731.017.204) of the research program Science PPP Fund, which is (partly) financed by the Dutch Research Council (NWO) in collaboration with ChemistryNL. We would like to thank our colleagues in the LocalBioFood consortium for the fruitful discussions.

Appendix A. Supporting information

Supplementary data associated with this article can be found in the online version at doi:10.1016/j.foostr.2023.100352.

References

Aguilera, J. M. (2005). Why food micro structure? *Journal of Food Engineering, 67*(1–2), 3–11. https://doi.org/10.1016/j.jfoodeng.2004.05.050

Ako, K., Durand, D., Nicolai, T., & Becu, L. (2009). Quantitative analysis of confocal laser scanning microscopy images of heat-set globular protein gels. *Food Hydrocolloids, 23*(4), 1111–1119. https://doi.org/10.1016/j.foodhyd.2008.09.003

Ayala-Hernandez, I., Goff, H. D., & Corredig, M. (2008). Interactions between milk proteins and exopolysaccharides produced by Lactococcus lactis observed by scanning electron microscopy. *Journal of Dairy Science, 91*(7), 2583–2590. https://doi.org/10.3168/jds.2007-0876

Babella, G. (1989). Scientific and practical results with use of ultrafiltration in Hungary. *International Dairy Federation, 244*, 7–24.

Birch, J., Van Calsteren, M. R., Pérez, S., & Svensson, B. (2019). The exopolysaccharide properties and structures database: EPS-DB. Application to bacterial exopolysaccharides. *Carbohydrate Polymers, 205*, 565–570. https://doi.org/10.1016/j.carbpol.2018.10.063

Buldo, P., Benfeldt, C., Carey, J. P., Folkenberg, D. M., Jensen, H. B., Sieuwerts, S., Vlachvei, K., & Ipsen, R. (2016). Interactions of milk proteins with low and high acyl gellan: Effect on microstructure and textural properties of acidified milk. *Food Hydrocolloids, 60*, 225–231. https://doi.org/10.1016/j.foodhyd.2016.03.041

Cheng, K., Zhou, Y., & Neelamegham, S. (2017). DrawGlycan-SNFG: A robust tool to render glycans and glycopeptides with fragmentation information. *Glycobiology, 27*(3), 200–205. https://doi.org/10.1093/glycob/cww115

Corredig, M., Sharafbafi, N., & Kristo, E. (2011). Polysaccharide-protein interactions in dairy matrices, control and design of structures. *Food Hydrocolloids, 25*(8), 1833–1841. https://doi.org/10.1016/j.foodhyd.2011.05.014

Dalgleish, D. G. (2011). On the structural models of bovine casein micelles - Review and possible improvements. *Soft Matter, 7*(6), 2265–2272. https://doi.org/10.1039/c0sm00806k

Dalgleish, D. G., & Corredig, M. (2012). The structure of the Casein Micelle of milk and its changes during processing. *Annual Review of Food Science and Technology, 3*(1), 449–467. https://doi.org/10.1146/annurev-food-022811-101214

de Jong, S., & van de Velde, F. (2007). Charge density of polysaccharide controls microstructure and large deformation properties of mixed gels. *Food Hydrocolloids, 21*(7), 1172–1187. https://doi.org/10.1016/j.foodhyd.2006.09.004

Duboc, P., & Mollet, B. (2001). Applications of exopolysaccharides in the dairy industry. *International Dairy Journal, 11*(9), 759–768. https://doi.org/10.1016/S0958-6946(01)00119-4

Egorov, S. A. (2022). Depletion interactions between nanoparticles: The effect of the polymeric depletant stiffness. *Polymers, 14*(24). https://doi.org/10.3390/polym14245398

Everett, D. W., & McLeod, R. E. (2005). Interactions of polysaccharide stabilisers with casein aggregates in stirred skim-milk yoghurt. *International Dairy Journal, 15*(11), 1175–1183. https://doi.org/10.1016/j.idairyj.2004.12.004

Fenoul, F., Le Denmat, M., Hamdi, F., Cuvelier, G., & Michon, C. (2008). Technical note: Confocal scanning laser microscopy and quantitative image analysis: Application to cream cheese microstructure investigation. *Journal of Dairy Science, 91*(4), 1325–1333. https://doi.org/10.3168/jds.2007-0531

Gentès, M. C., St-Gelais, D., & Turgeon, S. L. (2013). Exopolysaccharide-milk protein interactions in a dairy model system simulating yoghurt conditions. *Dairy Science and Technology, 93*(3), 255–271. https://doi.org/10.1007/s13594-013-0121-x

Girard, M., & Schaffer-Lequart, C. (2008). Attractive interactions between selected anionic exopolysaccharides and milk proteins. *Food Hydrocolloids, 22*(8), 1425–1434. https://doi.org/10.1016/j.foodhyd.2007.09.001

Glover, Z. J., Ersch, C., Andersen, U., Holmes, M. J., Povey, M. J., Brewer, J. R., & Simonsen, A. C. (2019). Super-resolution microscopy and empirically validated autocorrelation image analysis discriminates microstructures of dairy derived gels. *Food Hydrocolloids, 90*, 62–71. https://doi.org/10.1016/j.foodhyd.2018.12.004

Hassan, A. N. (2008). ADSA foundation scholar award: Possibilities and challenges of exopolysaccharide-producing lactic cultures in dairy foods. *Journal of Dairy Science, 91*(4), 1282–1298. https://doi.org/10.3168/jds.2007-0558

Hege, J., Palberg, T., & Vilgis, T. A. (2020). Interactions of different hydrocolloids with milk proteins. *JPhys Materials, 3*(4). https://doi.org/10.1088/2515-7639/aba2b7

Hemar, Y., Tamehana, M., Munro, P. A., & Singh, H. (2001). Viscosity, microstructure and phase behavior of aqueous mixtures of commercial milk protein products and xanthan gum. *Food Hydrocolloids, 15*(4–6), 565–574. https://doi.org/10.1016/S0268-005X(01)00077-7

Jamil, T., Gissinger, J. R., Garley, A., Saikia, N., Upadhyay, A. K., & Heinz, H. (2019). Dynamics of carbohydrate strands in water and interactions with clay minerals: Influence of pH, surface chemistry, and electrolytes. *Nanoscale, 11*(23), 11183–11194. https://doi.org/10.1039/c9nr01867k

Kayitmazer, A. B., Seyrek, E., Dubin, P. L., & Staggemeier, B. A. (2003). Influence of chain stiffness on the interaction of polyelectrolytes with oppositely charged micelles and proteins. *Journal of Physical Chemistry B, 107*(32), 8158–8165. https://doi.org/10.1021/jp034065a

Kruif, C. G. De, & Tuinier, R. (2001). *Polysaccharide Protein interactions, 15*, 555–563.

Laneuville, S. I., & Turgeon, S. L. (2014). Microstructure and stability of skim milk acid gels containing an anionic bacterial exopolysaccharide and commercial polysaccharides. *International Dairy Journal, 37*(1), 5–15. https://doi.org/10.1016/j.idairyj.2014.01.014

Loeffler, M., Hilbig, J., Velasco, L., & Weiss, J. (2020). Usage of in situ exopolysaccharide-forming lactic acid bacteria in food production: Meat products—A new field of application? *Comprehensive Reviews in Food Science and Food Safety, 19*(6), 2932–2954. https://doi.org/10.1111/1541-4337.12615

Lucey, J. A., & Singh, H. (1997). Formation and physical properties of acid milk gels: A review. *Food Research International, 30*(7), 529–542. https://doi.org/10.1016/S0963-9969(98)00015-5

Lucey, John A. (2004). Cultured dairy products: An overview of their gelation and texture properties. *International Journal of Dairy Technology, 57*(2–3), 77–84. https://doi.org/10.1111/j.1471-0307.2004.00142.x

Lynch, K. M., Zannini, E., Coffey, A., & Arendt, E. K. (2018). Lactic acid bacteria exopolysaccharides in foods and beverages: Isolation, properties. *Characterization, and Health Benefits*.

Marguerite, R. (2001). Relation between the molecular structure of some polysaccharides and original properties in sol and gel states. *Food Hydrocolloids, 15*(4–6), 433–440.

Mende, S., Rohm, H., & Jaros, D. (2016). Influence of exopolysaccharides on the structure, texture, stability and sensory properties of yoghurt and related products. *International Dairy Journal, 52*, 57–71. https://doi.org/10.1016/j.idairyj.2015.08.002

Metilli, L., Francis, M., Povey, M., Lazidis, A., Stephanie, M.-T., Ray, J., & Simone, E. (2020). Latest advances in imaging techniques for characterizing soft, multiphasic food materials. *Advances in Colloid and Interface Science, 2019*, Article 104265. https://doi.org/10.1016/j.meegid.2020.104265

Morris, G. A., Patel, T. R., Picout, D. R., Ross-Murphy, S. B., Ortega, A., Garcia de la Torre, J., & Harding, S. E. (2008). Global hydrodynamic analysis of the molecular flexibility of galactomannans. *Carbohydrate Polymers, 72*(2), 356–360. https://doi.org/10.1016/j.carbpol.2007.08.017

Pugnaloni, L. A., Matia-Merino, L., & Dickinson, E. (2005). Microstructure of acid-induced caseinate gels containing sucrose: Quantification from confocal microscopy and image analysis. *Colloids and Surfaces B: Biointerfaces, 42*(3–4), 211–217. https://doi.org/10.1016/j.colsurfb.2005.03.002

Rinaudo, M., & Milas, M. (2000). Gellan gum, a bacterial gelling polymer. *Developments in Food Science, 41*(C), 239–263. https://doi.org/10.1016/S0167-4501(00)80012-6

Robertson, C. (2012). Theory and practical recommendations for autocorrelation-based image correlation spectroscopy. *Journal of Biomedical Optics, 17*(8), Article 080801. https://doi.org/10.1117/1.jbo.17.8.080801

Savaiano, D. A., & Hutkins, R. W. (2021). Yogurt, cultured fermented milk, and health: A systematic review. *Nutrition Reviews, 79*(5), 599–614. https://doi.org/10.1093/nutrit/nuaa013

Schefer, L., Adamcik, J., & Mezzenga, R. (2014). Unravelling secondary structure changes on individual anionic polysaccharide chains by atomic force microscopy. *Angewandte Chemie - International Edition, 53*(21), 5376–5379. https://doi.org/10.1002/anie.201402855

Silva, J. V. C., Legland, D., Cauty, C., Kolotuev, I., & Floury, J. (2015). Characterization of the microstructure of dairy systems using automated image analysis. *Food Hydrocolloids, 44*, 360–371. https://doi.org/10.1016/j.foodhyd.2014.09.028

Sodini, I., Remeuf, F., Haddad, C., & Corrieu, G. (2004). The relative effect of milk base, starter, and process on yogurt texture: A review. *Critical Reviews in Food Science and Nutrition, 44*(2), 113–137. https://doi.org/10.1080/10408690490424793

Sone, I., Hosoi, M., Geonzon, L. C., Jung, H., & Bernadette, F. (2022). Gelation and network structure of acidified milk gel investigated at different length scales with and without addition of iota -carrageenan. September 2021 *Food Hydrocolloids, 123*, Article 107170. https://doi.org/10.1016/j.foodhyd.2021.107170.

Super, B. J., & Bovik, A. C. (1991). Localized measurement of image fractal dimension using gabor filters. *Journal of Visual Communication and Image Representation, 2*(2), 114–128. https://doi.org/10.1016/1047-3203(91)90002-W

Sworn, G., & Stouby, L. (2021). *Gellan gum. In Handbook of Hydrocolloids* (3rd ed..,). Elsevier Ltd. https://doi.org/10.1016/b978-0-12-820104-6.00009-7

Syrbe, A., Bauer, W. J., & Klostermeyer, H. (1998). Polymer science concepts in dairy systems - An overview of milk protein and food hydrocolloid interaction. *International Dairy Journal, 8*(3), 179–193. https://doi.org/10.1016/S0958-6946(98)00041-7

Tamang, J. P., Cotter, P. D., Endo, A., Han, N. S., Kort, R., Liu, S. Q., Mayo, B., Westerik, N., & Hutkins, R. (2020). Fermented foods in a global age: East meets West. *Comprehensive Reviews in Food Science and Food Safety, 19*(1), 184–217. https://doi.org/10.1111/1541-4337.12520

Tan, Y. L., Ye, A., Singh, H., & Hemar, Y. (2007). Effects of biopolymer addition on the dynamic rheology and microstructure of renneted skim milk systems. *Journal of Texture Studies, 38*(3), 404–422. https://doi.org/10.1111/j.1745-4603.2007.00104.x

Tiwari, S., Kavitake, D., Devi, P. B., & Halady Shetty, P. (2021). Bacterial exopolysaccharides for improvement of technological, functional and rheological

properties of yoghurt. *International Journal of Biological Macromolecules, 183*, 1585–1595. https://doi.org/10.1016/j.ijbiomac.2021.05.140

Tong, K., Xiao, G., Cheng, W., Chen, J., & Sun, P. (2018). Large amplitude oscillatory shear behavior and gelation procedure of high and low acyl gellan gum in aqueous solution. *Carbohydrate Polymers, 199*(July), 397–405. https://doi.org/10.1016/j.carbpol.2018.07.043

Torres, I. C., Amigo Rubio, J. M., & Ipsen, R. (2012). Using fractal image analysis to characterize microstructure of low-fat stirred yoghurt manufactured with microparticulated whey protein. *Journal of Food Engineering, 109*(4), 721–729. https://doi.org/10.1016/j.jfoodeng.2011.11.016

Tuinier, R., Van Casteren, W. H. M., Looijesteijn, P. J., Schols, H. A., Voragen, A. G. J., & Zoon, P. (2001). Effects of structural modifications on some physical characteristics of exopolysaccharides from Lactococcus lactis. *Biopolymers, 59*(3), 160–166. https://doi.org/10.1002/1097-0282(200109)59:3<160::AID-BIP1015>3.0.CO;2-V

Turgeon, S. L., & Laneuville, S. I. (2009). Protein + Polysaccharide Coacervates and Complexes. From Scientific Background to their Application as Functional Ingredients in Food Products. *Modern Biopolymer Science (First Edit)*. Elsevier Inc,. https://doi.org/10.1016/B978-0-12-374195-0.00011-2

Weinbreck, F., Nieuwenhuijse, H., Robijn, G. W., & De Kruif, C. G. (2003). Complex formation of whey proteins: Exocellular polysaccharide EPS B40. *Langmuir, 19*(22), 9404–9410. https://doi.org/10.1021/la0348214

Williams, P. A., & Phillips, G. O. (2003). The use of hydrocolloids to improve food texture. In *Texture in Food* (Vol. 1). Woodhead Publishing Limited. https://doi.org/10.1533/9781855737082.2.251

Zdunek, A., & Pieczywek, P.M. (2021). The primary, secondary, and structures of higher levels of pectin polysaccharides. September 2020, 1101–1117. https://doi.org/10.1111/1541–4337.12689.

Zhang, L., Folkenberg, D. M., Amigo, J. M., & Ipsen, R. (2016). Effect of exopolysaccharide-producing starter cultures and post-fermentation mechanical treatment on textural properties and microstructure of low fat yoghurt. *International Dairy Journal, 53*, 10–19. https://doi.org/10.1016/j.idairyj.2015.09.008

Zhang, L., Folkenberg, D. M., Qvist, K. B., & Ipsen, R. (2015). Further development of a method for visualisation of exopolysaccharides in yoghurt using fluorescent conjugates. *International Dairy Journal, 46*, 88–95. https://doi.org/10.1016/j.idairyj.2014.08.018